Steady state HiPIMS discharge optimization through the control of the magnetic field

J. Čapek, M. Hála, O. Zabeida, J.E. Klemberg-Sapieha, and L. Martinu[a]

Department of Engineering Physics, École Polytechnique de Montréal,

P.O. Box 6079, Station Downtown, Montreal, Quebec H3C 3A7,

Canada

(Dated: 12 August 2011)

High power impulse magnetron sputtering (HiPIMS) is a pulsed DC sputtering technique utilizing high power density peaks of typically more than $100 \, \mathrm{W \, cm^{-2}}$. The discharge operation at such elevated powers can be hindered by the magnetron configuration (size and magnetic field) and/or the target conditions (e.g. material and thickness). In addition, target erosion is an important issue significantly affecting process reproducibility. In the present work, we propose a simple approach for the stabilization of the HiPIMS discharge by controlling the target magnetic field using paramagnetic spacers with different thicknesses in between the magnetron surface and the target. We demonstrate a straightforward discharge optimization, while using various target materials, such as Nb, Ta, Cr, Al, Ti, Si, and even C (graphite). The existence of a steady state high density discharge above the graphite target and the other targets in general is discussed in terms of the magnetic field configuration and the gas rarefaction effect.

[a]ludvik.martinu@polymtl.ca

I. INTRODUCTION

High power impulse magnetron sputtering (HiPIMS) is a pulsed DC sputtering technique utilizing high power density peaks of typically more than $100\,\mathrm{W\,cm^{-2}}$ at sufficiently low time-averaged power density in order to avoid target overheating. This results in a high density discharge and, consequently, in a high degree of ionization of the sputtered material. This makes HiPIMS a very attractive deposition technique for enhancing and tailoring coating properties.[1,2]

Recently, Anders *at al.* described[3] that specific conditions have to be met in order to reach a high density (HD) discharge. Probably, the most important criterion is the sufficiently high pulse voltage value, U_c. If U_c is lower than a certain threshold, U_{th}, a low density (LD) discharge is observed [see Fig. 1 (dotted line)], such as in DC magnetron sputtering (DCMS).

At time $t = 0\,\mathrm{\mu s}$, the target is surrounded only by Ar atoms at a preset pressure, thus the initial current density growth can be mostly attributed to Ar ions impacting on the target. However, the sputtered atoms transfer their momentum through collisions to the surrounding gas. This results in a heating and consequently in a rarefaction of the Ar atoms.[4] It is to be noted that a similar effect can also be caused by an elevated temperature of the target surface.[5] Since Ar ions are the only particles which are able to generate secondary electrons (SE) in LD plasma,[3] the discharge current density starts to decrease at some point to a steady state value reached after several tens of microseconds. The resulting current density is mainly determined by the reduced concetration of Ar atoms close to the target surface.[6]

For U_c higher than U_{th} [Fig. 1 (solid line)] the number and the energy of SE are sufficient to ionize an important fraction of the sputtered atoms. The target ion can then be attracted back to the target by the large potential fall across the plasma (pre)sheath. Although the rarefaction of the working gas is even more pronounced at higher powers, the back-attracted excited target ions, and especially the doubly ionized target atoms, are able to partially substitute the role of Ar ions in the generation of the SE.[7,8] The latter process is crucial for sustaining the HD discharge. As a consequence, the HD discharge reaches a steady state, which is characterized by a substantially higher value of the current density compared to the LD case.
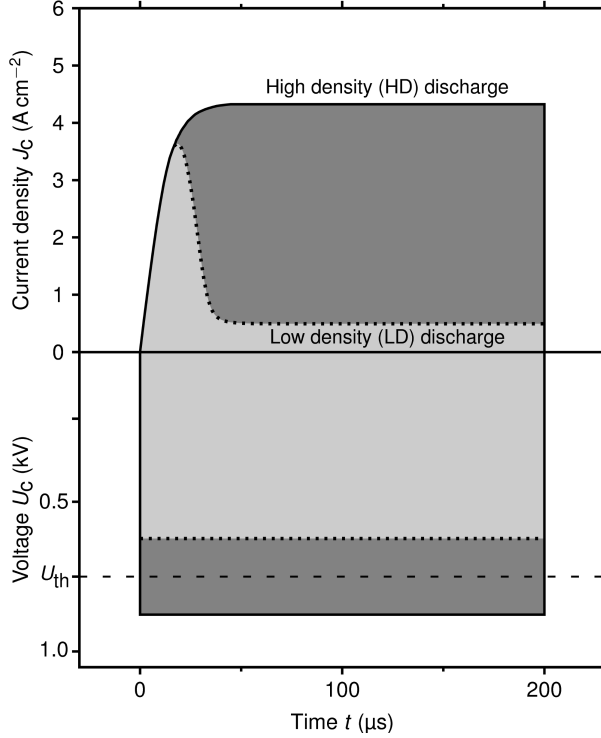
FIG. 1. Schematic waveforms of the pulse voltage U_c and the target current density, J_c, for a case that $U_c < U_{th}$ (dotted line) and $U_c > U_{th}$ (solid line), where U_{th} is a threshold for the high density plasma (dashed line).

In some specific conditions, the ions of the sputtered material are able to take over the role of the Ar ions completely, thus the background Ar gas can be omitted without loosing the HD discharge regime.[9–11] The condition for such a mode, termed "sustained self sputtering", or "gasless sputtering", was originally introduced by Hosokawa[12] *at al.* as

$$\Pi \equiv \alpha\,\beta\,\gamma_{ss} = 1, \tag{1}$$

where, α is the probability that a sputtered atom becomes ionized, β is the probability that the newly formed ion returns to the target, and, γ_{ss} is the self sputtering yield. Since $\alpha < 1$ and $\beta < 1$, it is necessary that $\gamma_{ss} > 1$. One of the advantages of such a HD discharge is the deposition of dense coatings without any contamination by the working gas. However, an additional source of metal ions (e.g. pulsed cathodic arc[11]) is needed to initiate the discharge at every high voltage pulse.

Despite of the effort that has been devoted to the understanding of the HiPIMS processes in the last years, its practical implementation may be complicated due to several types of

3

problems: (i) HiPIMS power supply overloading, (ii) excessive arcing, and (iii) strong effect of target erosion. In the present work, we discuss in more detail on the above issues, and we propose a straightforward solution based on the magnetron's magnetic field control. In addition, we demonstrate the significance of the gas rarefaction effect on the HiPIMS discharges by providing the experimental evidence for various target materials, including those with a low sputtering yield such as carbon (graphite).

II. EXPERIMENTAL SETUP

All experiments were performed in a vacuum deposition system illustrated in Fig. 2 using a grounded stainless steel chamber, in a pure Ar atmosphere, and a pressure, $p = 1\,\mathrm{Pa}$. An unbalanced magnetron (5 cm in diameter) was powered by a HÜTTINGER Electronics
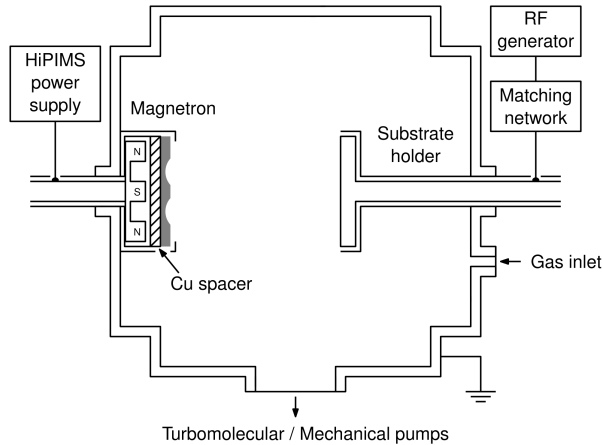

FIG. 2. Schematic diagram of the experimental setup.

HMP2/1 power supply (2 kW maximum average power) working in the frequency range from 2 to 500 Hz, at a voltage pulse duration between 1 and 200 µs and with a maximum voltage and peak current of 2 kV and 1000 A, respectively. A repetition frequency $f_\mathrm{r} = 50\,\mathrm{Hz}$ and a pulse duration $t_\mathrm{p} = 200\,\mathrm{\mu s}$ were used in order to be able to reach a steady state HD discharge without overheating the magnetron. We intentionally used such a small-size magnetron since it allowed us to achieve very high power densities during the pulses at lower total (average) powers.

The magnetron's magnetic field is shown in Fig. 3. This measurement of the field distribution was performed by a home-made mapping system where the position of a LakeShore

HMNT-4E04-VR Hall probe was controlled by a x–y movable stage. More details concerning the measurement and properties of the magnetic field are presented in Appendix A. The substrate holder (surface area $\sim 50\,\mathrm{cm}^2$; target-to-substrate distance $d = 10\,\mathrm{cm}$) was biased at a low power ($\sim 10\,\mathrm{W}$) to obtain a negative bias voltage of $-20\,\mathrm{V}$ by an additional RF power supply in order to facilitate the discharge ignition.

In this work, different target materials have been tested; this includes: Ta, Nb, Cr, Ti, Al (6.35 mm thick), n-doped Si (total thickness 3.18 mm Si + 3.18 mm copper bonding), and C–graphite (3.18 mm thick). Copper spacers placed in between the target and the magnetron head were used to modify the magnetic field strength. The thickness, d_s, of the spacers was in the range of 0 to 5 mm. The target erosion was measured as a ratio between the depth of target erosion in the race track center and the thickness of a new target.

Waveforms of the cathode voltage and discharge current were measured by a Tektronix P6015A voltage probe and a Pearson 301X current monitor, respectively, and recorded by a Tektronix TDS2014B digital oscilloscope.

Optical emission from the discharge was collected by an optical fibre probe mounted within the reactor overlooking the discharge at a distance of $d \approx 1\,\mathrm{cm}$ parallel with the target surface. The time-averaged optical spectra were analyzed by Ocean Optics USB2000 spectrometer.

III. COMMON ISSUES IN THE HIPIMS PROCESS IMPLEMENTATION

In this section we discuss various general problems related to the implementation of a HiPIMS discharge in deposition systems; this includes HiPIMS power supply overloading, excessive arcing, and the strong effect of target erosion. Possible solutions are also outlined.

A. HiPIMS power supply overloading

The steady state HD discharge (depicted in Fig. 1) can be reached only in the case when the HiPIMS power supply can sustain a constant voltage ($U_\mathrm{c} > U_\mathrm{th}$) during the whole pulse. If the resulting HD discharge current value is too high (due to a large target surface, a strong magnetron's magnetic field or a high emission of SE from the target) the steady state cannot be reached. Instead, a peak-shaped current waveform is observed (as exemplified Fig. 4).
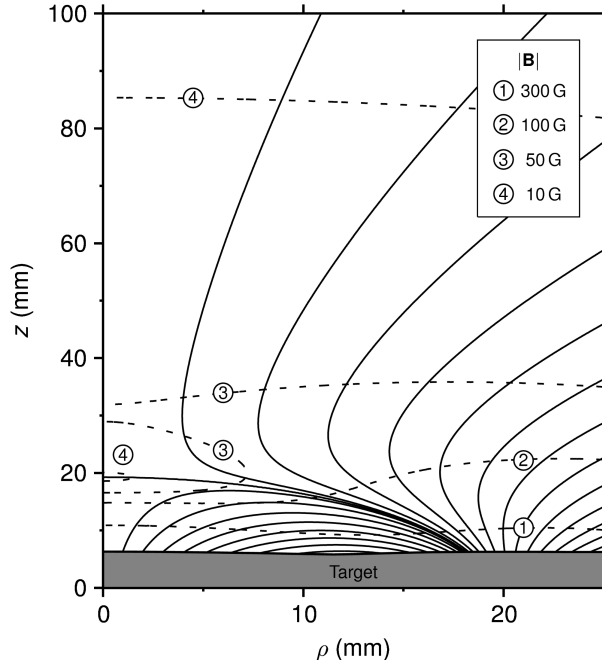
FIG. 3. Magnetic field lines (solid lines) and contours of the magnetic field, $|\mathbf{B}|$, (dashed lines) corresponding to the magnetic field of the 50 mm diameter unbalanced magnetron used in this work.

Here, high current values at the beginning of the pulse significantly reduce the charge stored in the pulse unit capacitors of the HiPIMS power supply. As a consequence, the U_c starts to decrease at $t_1 = 30\,\mu s$ (as indicated by the time line no. 1 in Fig. 4), followed by the U_c maximum, and consequently by the drop of the HD current. Moreover, beyond $t_2 = 130\,\mu s$ (time line no. 2) an even more rapid fall of the current is observed. The latter effect is caused by a voltage drop below the voltage threshold for the sustained HD discharge.[13]

It should be highlighted that due to the power supply overloading neither the voltage nor the current levels are stable. This complicates understanding and modeling of the discharge.

B. Excessive arcing

The number and the energy of the emitted SE are very important discharge parameters. Furthermore, the production mechanism of the SE is crucial as well. A typical discharge in plasma processing is operated in a glow or an abnormal glow discharge regime where the SE are individually emitted by the impacting ions. However, the HiPIMS process is characterized by a high target ion current density, J_{ci}, that narrows the sheath thickness, x_c,
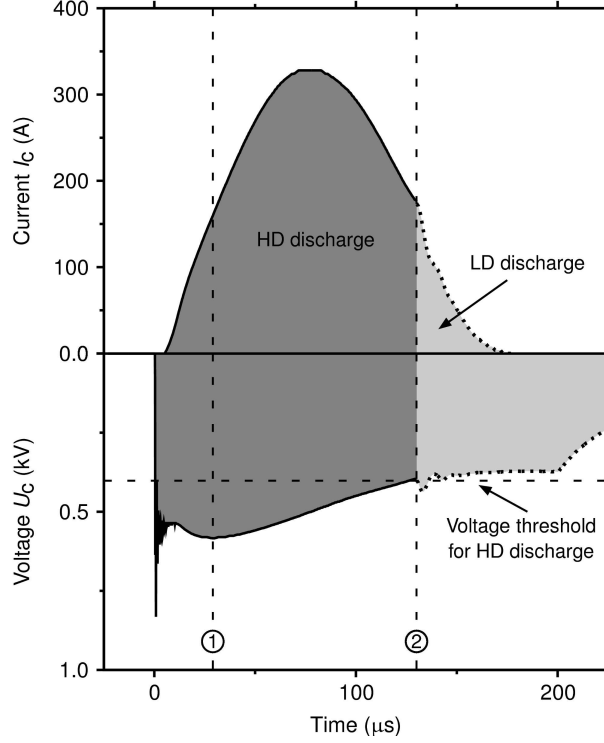
FIG. 4. Waveforms of the magnetron voltage U_c and the target current, I_c, for a Ti target. The line no. 1 denotes the time at which the pulse voltage starts to decrease because of insufficient charge stored in the pulse unit capacitors of the HiPIMS power supply. The line no. 2 represents the time at which the HD discharge is lost due to the drop of the voltage under a threshold for HD plasma.

accordingly to the Child's law. For instance, the collisionless Child's law results in a sheath thickness $x_{c,DCMS} = 300\,\mu m$ for a typical DCMS discharge ($J_{ci} = 50\,mA\,cm^{-2}$, $U_c = 0.3\,kV$) and $x_{c,HiPIMS} = 45\,\mu m$ for a typical HiPIMS discharge ($J_{ci} = 4\,A\,cm^{-2}$, $U_c = 0.6\,kV$) above a Nb target. The thinner sheath significantly increases the electrical field intensity, E, close to the target surface from $E_{DCMS} = 1.0 \times 10^6\,V\,m^{-1}$ to $E_{HiPIMS} = 1.3 \times 10^7\,V\,m^{-1}$. Such a rise in E may substantially enhance the probability of electron field emission at target defects (i.e. grain boundaries, inclusions).[14] Hence, HiPIMS discharge is much more prone to a transition to the collective field and thermal electron emission regimes. In such a case, the large scale discharge collapses into a small cathodic spot through which a high current density may flow. The latter discharge is known as an arc.

Arcing during the deposition process is a serious issue. Despite the fact that arc handling is now a standard feature of commercial HiPIMS power supplies, there can be some residual

energy in the discharge circuit even after the arc detection. This may lead to the ejection of macroparticles from the sputtered target, and thus to a possible deterioration of the coating quality.

C. Strong effect of target erosion

Figure 5 shows the steady state current as a function of the pulse voltage for different erosion states (6 and 80 %) of a Nb target. Transition from the LD to the HD discharge is characterized by a jump in the current, and consequently by a change in the curve slope.[15,16] Interestingly, a zero or even a negative slope can be observed during the HD discharge for some combinations of the magnetron's magnetic field configuration and the target material (see Fig. 5). One possible explanation of the observed flattening of the I–V curve is a lower SE confinement by the magnetic field of the magnetron at elevated voltage values.[15,17] As a result, a significant portion of these electrons will be lost without contributing to the plasma density. This effect may be further enhanced by an increased magnetic deconfinement due to the rise of the Hall current upon a transition from the LD to the HD regime.[18,19]

This phenomenon is not a problem by itself, but it will negatively affect the long-term reproducibility (e.g. the constant deposition rate) of the deposition process. As illustrated in Figure 5, the progressing target erosion can result in a substantial rise of the HD current level. In such a situation, it is impossible to reach the original (low level) current without a loss of the HD discharge. Consequently, the deposition conditions are irreversibly altered.
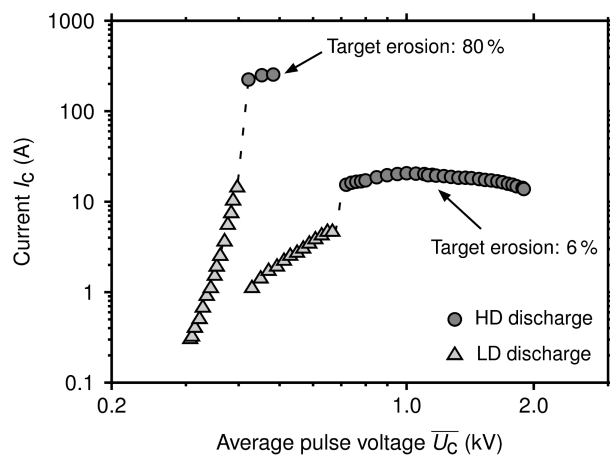

FIG. 5. Current–voltage characteristics corresponding to different erosion states (6 and 80 %) of the Nb target.

8

D.   Possible solutions

The difficulties with the application and implementation of the HiPIMS described above indicate a need for process optimization. An adequate solution should permit: (i) to sustain the HD discharge during most of the duration of the HiPIMS pulse, (ii) to minimize arcing, and (iii) to enhance the process reproducibility.

A possible answer to the above requirements is the ability to adjust the current level during the HD discharge. This may be performed by the modification of the magnetron's magnetic field by one of the following approaches: (i) use of a magnetron equipped by electromagnets,[10] (ii) replacement of the permanent magnets inside the magnetron,[20] (iii) application of an external magnetic field (i.e. additional coil[21] or permanent magnets[22]), or (iv) adjustment of the distance between the target surface and the permanent magnets.[23] In this work, we utilize the latter approach by inserting paramagnetic (copper) spacers of different thicknesses between the target and the magnetron head.

IV.   OPTIMIZATION OF THE HIGH DENSITY DISCHARGE

In this section we study the effect of the target erosion on the HiPIMS discharge characteristics above the Nb target for the case when the HD current level is independent of the pulse voltage. We then demonstrate application of the copper spacers for control of the magnetic field and the consequent steady state HD discharge optimization. Finally, we present model examples of the optimized HiPIMS discharge for Ta, Cr, Al, Ti, Si, and C targets.

A.   Control of the HiPIMS discharge through the optimization of the magnetic field

The HiPIMS discharge characteristics in front of the Nb target depend on the level of target erosion and on the thickness of the inserted spacer. The distribution of the radial component, $|B_\rho|$, of the magnetic field around the Nb target at different stages of erosion is illustrated in Fig. 6. The corresponding current waveforms for various preset voltages are shown in Figure 7 (a $-$ c).

For a low target erosion of 6 %, a radial magnetic field at the target surface $B_\rho = 550\,\mathrm{G}$ (Fig. 6) and a racetrack area $A_\mathrm{r} = 9.3\,\mathrm{cm}^2$ lead to a typical LD discharge for pulse voltages

$U_c < U_{th} = 0.7\,\text{kV}$ [Fig. 7 (a)]. Pulse voltages higher than this U_{th} threshold result in a steady state HD discharge at a maximum current value of approximately 20 A at $U_c = 1\,\text{kV}$. Surprisingly, the HD current does not rise even for very high voltages, (e.g. $U_c > 1\,\text{kV}$). Instead, we observe a slow decrease of the steady state HD current level to 14 A at $U_c = 2\,\text{kV}$, such as previously illustrated in Fig. 5. This behavior can probably be attributed to an enhanced energy of the SE at these voltages, as previously discussed in section III C.
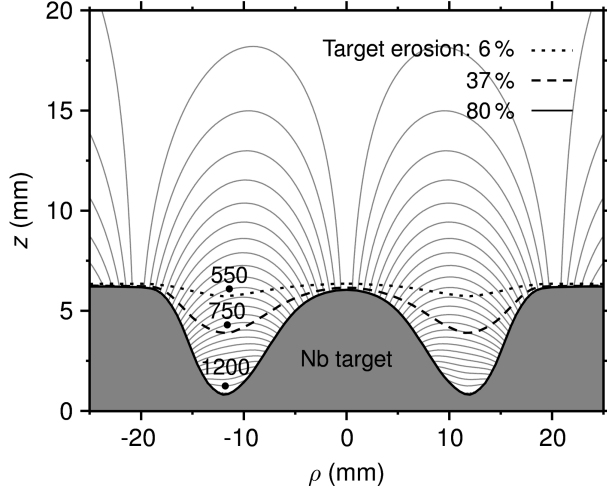

FIG. 6. Niobium target profiles at different erosion states (6, 37, and 80 %) presented together with the absolute values of the radial component $|B_\rho|$ of the magnetron's magnetic field (in Gauss).

The discharge behavior at a target erosion of 37 % [Fig. 7 (b)] is similar to the previous case. Clearly, a stronger magnetic field $B_\rho = 750\,\text{G}$ (Fig. 6) and a larger surface of the race-track $A_r = 11.9\,\text{cm}^2$ lead to a higher current level. For instance, the steady state value of the HD discharge current at $U_c = 1.0\,\text{kV}$ is 53 A in this case. Moreover, the HD plasma threshold U_{th} decreases from 0.7 to 0.6 kV. In these experiments, voltages higher than 1.4 kV cannot be used in order to avoid overheating the magnetron.

For a high target erosion of 80 % the magnetic field is about two times stronger ($B_\rho = 1200\,\text{G}$ in Fig. 6) and the surface area 50% larger ($A_r = 15.1\,\text{cm}^2$) as compared to the new target. These conditions lead to a low voltage threshold $U_{th} = 0.5\,\text{kV}$ and give rise to large HD current peaks reaching a maximum value of up to 215 A at $U_c = 0.6\,\text{kV}$ (the maximum voltage that can be applied without the magnetron overheating) [Fig. 7 (c)]. These elevated discharge current values lead to power supply overloading and a higher probability of arc development (section III).

10

Since the high density current is independent of the pulse voltage it is necessary to decrease the magnetic field strength in order to reproduce the desired steady state HD discharge. This has been accomplished by the introduction of a metallic (Cu) spacer in between the target and the magnetron that allows one to effectively compensate the effects of the stronger magnetic field and the larger surface area of the racetrack. As an example, the modification of the discharge characteristics for the highly eroded target (80 %) is demonstrated with the application of three different spacers with thicknesses $d_s = 1.7$, 3.4, and 5.0 mm [Fig. 7 (d)–(f)].

For $d_s = 1.7$ and 3.4 mm, a stable HD discharge is obtained even for a highly eroded target. It should be stressed that the HD discharge currents for $d_s = 3.4$ are similar to the current levels obtained for a new or slightly eroded target. However, some minor differences in the shape of the current waveforms can be noted, particularly during the first 20 µs of the pulse. This effect may be explained by the modified surface and shape of the racetrack (erosion state 80 % vs 6 %), and the related gas dynamics. When the resulting magnetic field is too weak (spacer thickness $d_s = 5.0$ mm) the transition to the HD discharge is inhibited due to a low SE confinement.

Figure 8 shows the obtained steady state current for a fixed $U_c = 0.8$ kV as a function of the magnetic field strength (spacer thickness). The decreasing current level illustrates the strong effect of the magnetic field on the HD discharge current [Fig. 8 (a)]. Subsequently, different discharge regimes (e.g. "Stable HD discharge", "Transition to LD discharge", and "Stable LD discharge") can be identified as illustrated in Fig. 8 (b).

One can clearly see, that the HD discharge current can be adjusted within a large range of values spanning from 105 A down to 14 A. This demonstrates the possibility to operate the HD discharge at low currents, and hence to eliminate and avoid the problems discussed in section III.

In addition, the voltage threshold U_{th} simultaneously increases with the decreasing magnetic field, such as demonstrated in Fig. 9. Since the HD current (Fig. 8) is more sensitive to the magnetic field strength alteration than is U_{th} (Fig. 9), one has the option to effectively minimize the HD discharge power threshold, P_{th}, as well (see Fig. 9). This feature allows to avoid magnetron overheating at a given pulse length and repetition frequency.

B. Optimization of the HiPIMS discharge for various target materials

In the above section we have described the importance of the magnetic field on the steady state HD discharge for the specific case of a Nb target. In this section, we extend this work for the sputtering other target materials.

Figure 10 shows current waveforms of the HD discharges operated above various target materials (Ta, Cr, Al, Ti, Si, and C) for which the HD discharge current was minimized through the control of the magnetic field. The shape of the corresponding current waveforms varies significantly from one material to another, which indicates differences in the discharge dynamics.

The rectangular-shape current waveforms of the discharges above the Ta and Cr targets [Fig. 10 (a) and (b)] are very similar to those of the discharges above the Nb target [Fig. 7 (a)]. In these three cases, the optimization process was fairly simple and often unnecessary; for instance, for a new target, for which the steady state HD discharge currents were already low (e.g. 20 A). In contrast, the HD discharge above the Al, and especially the Ti targets [Fig. 10 (c) and (d)] requires a longer time ($\sim 100 \, \mu$s) to stabilize and reach steady state conditions. Moreover, the discharge optimization was more difficult, i.e., the reached minimum HD currents were ≈ 25 A and ≈ 35 A for the Al and the Ti targets, respectively. Surprisingly, the discharges above the Si and even the C targets [Fig. 10 (e) and (f)] were also operated in the steady state HD discharge, even though with a significant delay ($t \approx 50 \, \mu$s) of the HD current at the beginning of the pulse. In fact, for both of these materials, contrary to the previously discussed targets, it is essentially impossible to reach conditions for sustained self sputtering [Eq. (1)]. This is due to the low sputtering yield of these materials, for which $\gamma_{\mathrm{ss}} = 0.71$ for Si and $\gamma_{\mathrm{ss}} = 0.27$ for C targets at an ion energy of 1 keV.[24] Here, let us note that the optimization process of these two discharges was the most complicated and the least effective. Particularly, the C target required a very low magnetic field strength in order to avoid arc occurrences. Even then, the resulting minimum steady state HD current was still relatively high (≈ 65 A).

V. HIGH DENSITY DISCHARGE AND GAS RAREFACTION EFFECT

In the previous section we have demonstrated the optimization of a steady state HiPIMS discharge through the control of the magnetic field for various target materials. In this section we discuss in more detail the importance of the magnetic field configuration and the gas rarefaction effect on the HD discharge current level.

In order to better understand the HD discharges operated above the C target, and the other target materials in general, the plasma composition was investigated using optical emission spectroscopy (OES). Figure 11 shows the OES spectra recorded from the LD and HD discharges operated above Nb and C targets. The plasma emission is dominated by sputtered species in the case of Nb discharges. In addition, the HD spectra exhibit a substantially higher emission from the ionized Nb lines than the LD spectra, and also a much lower intensity of the Ar emission lines. This is a consequence of the significant Ar (39.95 amu) rarefaction by the high fluxes of heavy Nb atoms (92.91 amu), and of the self sputtering mechanism during which an important fraction of the sputtered material gets ionized.

In contrast, the spectra of the LD discharge above the C target exhibit only neutral Ar emission lines. The transition to the HD regime is then accompanied by a significant rise of the emission from the ionized Ar atoms. This observation provides evidence that Ar atoms play a dominant role in both LD and HD discharges. It should be noted that a similar observation of the dominant Ar ions emission was also detected in the steady state HiPIMS discharges operated above highly poisoned metal targets.[25]

The above results can be interpreted by the low sputtering yield and the low mass of C atoms (12.01 amu) that result in a lower level of working gas rarefaction, as compared to heavier elements with a high sputtering yield.[4] Moreover, Figure 11 (b) indicates that the transition from the LD to the HD discharge mode could be reached even in a Ar atmosphere without any contribution of the target material species. In fact, one can then define a criterion [similar to condition (1)] for such a steady state HD discharge, where the flux of sputtered atoms is neglected, as follows:

$$\Pi_{\mathrm{g}} \equiv \gamma_{\mathrm{se}}\, \kappa_{\mathrm{e\text{-}g}}\, \beta_{\mathrm{g}} = 1, \tag{2}$$

where γ_{se} is the ion induced yield of SE, $\kappa_{\mathrm{e\text{-}g}}$ is the number of ionization collisions per one emitted SE, and β_{g} is the probability that the newly formed Ar ion is attracted towards

13

the target. Since $\gamma_{\text{se}} \approx 0.1$ (for metals[26]) and $\beta_{\text{g}} < 1$, it is necessary that $\kappa_{\text{e-g}} \approx 10$. The quantity $\kappa_{\text{e-g}}$ can be further expressed in terms of specific discharge characteristics:

$$\kappa_{\text{e-g}} = n_{\text{g}}\,\sigma_{\text{e-g}}(E_{\text{e}})\,l(\mathbf{B}), \tag{3}$$

where n_{g} is the concentration of neutral Ar atoms close to the target surface, $\sigma_{\text{e-g}}$ is the cross section for ionization of the Ar atom by an impacting SE (function of the electron energy E_{e}), and l is the length of a lifetime trajectory of a SE (function of the magnetic field $\mathbf{B}$). In principle, the condition $\kappa_{\text{e-g}} \approx 10$ is not difficult to attain since l can be substantially increased by a suitable magnetic field configuration of the magnetron. If $\Pi_{\text{g}} > 1$, the discharge current rises significantly, indicative of the transition to the HD discharge. The progressing working gas ionization results in a drop of n_{g}, and perhaps in a diminished l (due to the superimposed Hall current that modifies the magnetic field configuration[18,19]). Consequently, this leads to a stabilization of the discharge current and the establishment of a steady state HD discharge ($\Pi_{\text{g}} = 1$), if neglecting the generation of multiply ionized Ar atoms. This model can explain the presented discharge behavior above the C target [Fig. 10 (f)], and specifically, the abundant emission originating from Ar ions in the HD discharge [Fig. 11 (b)].

It has been already mentioned in section IV B that the optimization (minimization) of the HD current through the control of the magnetic field was more difficult for some target materials. This observation indicates that the effect of the magnetic field on SE confinement is accompanied by another important effect that influences the final value of the steady state HD current. The latter phenomenon can be related to the atomic mass and sputtering yield of the target material, which are, in fact, the two fundamental parameters in Ar gas rarefaction (replacement) by a flux of sputtered material. In order to illustrate this assumption, the minimized steady state HD current was plotted in Fig. 12 as a function of the normalized Ar gas density, K, which is defined as

$$K = \frac{n_{\text{r}}}{n_0}, \tag{4}$$

where n_{r} is the reduced density of Ar atoms close to the target surface, and n_0 is the density of Ar atoms close to the wall of the system. The former quantity was calculated according to the model of Rossnagel,[4] as specified in detail in Appendix B.

The HD discharge current is largely affected by n_{r} because of the high potential energy of the Ar ions ($15.8\,\text{eV}$) in contrast to the majority of the sputtered material ions.[8] The correlation of the HD current level and of n_{r} (illustrated in Fig. 12) can thus be interpreted

14

by the Ar gas rarefaction effect: For low values of K (< 0.07), the Ar gas is highly diluted by the flux of the sputtered material, and an almost pure self sputtering discharge can be reached (Nb, Ta). When K is increased, the contribution of Ar ions to the resulting current is more significant, and the sputtering mechanism of the HD discharge is gradually transformed from the self sputtering mode to the gas sputtering mode (Si, C). This observation confirms that Ar gas rarefaction by the sputtered particles is an important material-dependent phenomenon which governs the HD current level. It should be also noted that an elevated target surface temperature during the high power pulse may also cause the Ar gas density rarefaction.[5] Nevertheless, this effect was neglected during the presented calculation of the reduced Ar gas density.

It has been already mentioned in Section I that in the HD discharge a portion of the sputtered target atoms is ionized, attracted back to the target, and eventually (if their potential energy is sufficiently high[8]) produce SE as well. Hence, the decrease in the SE production by the bombarding Ar ions can be partially or even completely compensated by the back-attracted ions, especially for the high sputtering yield target materials. Consequently, the measured HD current may be higher than the predicted theoretical value corresponding to the Ar ion fluxes.[6]

In a general case, the contribution of both gas sputtering and self sputtering mechanisms to the resulting HD discharge should be considered. Therefore, the condition for the steady state HD discharge dominated by Ar ions (Eq. 2) is not complete and should be combined with the condition for the self sputtering mode (Eq. 1). A general criterion for a transition from the LD to the HD discharge will be presented and discussed in more detail in a separate publication.[27]

VI. SUMMARY AND CONCLUSIONS

In this paper, we discussed the concept of optimization of HiPIMS discharges operated above different elemental targets [Ta, Nb, Cr, Al, Ti, Si, and C (graphite)]. First, we described various problems related to the HiPIMS discharge implementation in the deposition systems, such as (i) HiPIMS power supply overloading, (ii) excessive arcing, and (iii) strong effect of target erosion. Second, we proposed a simple approach for the HiPIMS discharge optimization based on the application of copper (paramagnetic) spacers in between the mag-

netron and the target. This technique was demonstrated on a example of the HD discharge above a 80 % eroded Nb target; It was shown that the level of the steady state HD current can be controlled in the range of 14 – 105 A. Furthermore, we demonstrated successful stabilization of the HD mode at the lowest accessible discharge current for different materials, including Si and C. The observation of a steady high current level above C, supported by optical emission spectroscopy monitoring, indicated the dominant role of Ar ions in HD discharges above low yield target materials. Finally, we offered a correlation between the gas rarefaction effect and the HD discharge current value.

ACKNOWLEDGMENTS

REFERENCES

[1] K. Sarakinos, J. Alami., and S. Konstantinidis, Surf. Coat. Technol. **204**, 1661 (2010).

[2] A. Ehiasarian, "Plasma surface engineering research and its practical applications," (Kerala, India, 2008) Chap. Fundamentals and applications of HIPIMS, p. 35.

[3] A. Anders, J. Andersson, and A. Ehiasarian, J. Appl. Phys. **102**, 113303 (2007).

[4] S. Rossnagel, J. Vac. Sci. Technol. A **6**, 19 (1988).

[5] A. Anders, Surf. Coat. Technol. **205**, S1 (2011).

[6] S. Rossnagel, J. Vac. Sci. Technol. A **6**, 223 (1988).

[7] J. Vlček and K. Burcalová, Plasma Sources Sci. Technol. **19**, 065010 (2010).

[8] A. Anders, Appl. Phys. Lett. **92**, 201501 (2008).

[9] W. Posadowski and Z. Radzimski, J. Vac. Sci. Technol. A **11**, 2980 (1993).

[10] S. Kadlec and J. Musil, Vacuum **47**, 307 (1996).

[11] J. Andersson and A. Anders, Appl. Phys. Lett. **92**, 221503 (2008).

[12] N. Hosokawa, T. Tsukada, and H. Kitahara, Proceedings of the Eighth International Vacuum Congress, Le Vide, Cannes, France, 11(1980).

[13]M. Hála, N. Viau, O. Zabeida, J. Klemberg-Sapieha, and L. Martinu, J. Appl. Phys. **107**, 043305 (2010).

[14]A. Anders, Thin Solid Films **502**, 22 (2006).

[15]A. Ehiasarian, R. New, W.-D. Münz, L. Hultman, U. Helmersson, and V. Kouznetsov, Vacuum **65**, 147 (2002).

[16]J. Alami, K. Sarakinos, G. Mark, and M. Wuttig, Appl. Phys. Lett. **89**, 154104 (2006).

[17]J. Thornton, J. Vac. Sci. Technol. **15**, 171 (1978).

[18]J. Bohlmark, U. Helmersson, M. VanZeeland, I. Axnäs, J. Alami, and N. Brenning, Plasma Sources Sci. Technol. **13**, 654 (2004).

[19]S. Abolmasov and A. Bizyukov, IEEE Trans. Plasma Sci. **33**, 1447 (2005).

[20]J. Sags, L. Fontana, and H. Maciel, Vacuum **85**, 705 (2011).

[21]I. Ivanov, P. Kazansky, L. Hultman, I. Petrov, and J.-E. Sundgren, J. Vac. Sci. Technol. A **12**, 314 (1994).

[22]J. Musil, K. Rusňák, V. Ježek, and J. Vlček, Vacuum **46**, 341 (1995).

[23]T. Nakamura, S. Kato, and H. Nishiyama, "Magnetron sputtering apparatus," (1982), US patent US4309266.

[24]W. Eckstein, *Sputtering by Particle Bombardment*, Vol. 110 (Springer Berlin / Heidelberg, 2007) pp. 33–187.

[25]M. Hála, J. Čapek, O. Zabeida, J. Klemberg-Sapieha, and L. Martinu, submitted to J. Phys. D(2011).

[26]D. Depla, S. Heirwegh, S. Mahieu, J. Haemers, and R. D. Gryse, J. Appl. Phys. **101**, 013301 (2007).

[27]A. Anders, J. Čapek, M. Hála, and L. Martinu, submitted to Phys. Rev. Lett.(2011).

[28]D. Meeker, *computer program: Finite Element Method Magnetics 4.2* (2009).

[29]I. Svadkovski, D. Golosov, and S. Zavatskiy, Vacuum **68**, 283 (2003).

[30]E. Clementi, D. Raimondi, and W. Reinhardt, J. Chem. Phys. **47**, 1300 (1967).

[31]J. Ziegler, J. Biersack, and M. Ziegler, *computer program: TRIM-2011* (2011).

APPENDIX A

The axial (B_z) and radial (B_ρ) components of the magnetic field $\mathbf{B}$ (Fig. 3) were measured in the central plane in front of the magnetron head assuming that the magnetic field is

axisymmetrical. The magnetron magnetic field was also simulated by using the finite element software package FEMM[28] and the resulting map was fitted to the experimental data of $\mathbf{B}$. This approach enables one to calculate the magnetic vector potential, $\mathbf{A}$, defined as:

$$\mathbf{B} = \nabla \times \mathbf{A} \tag{5}$$

and consequently, the magnetic field in an arbitrary point. In the general 3D case, $\mathbf{A}$ is a vector with three components. However, in the 2D planar and axisymmetric case, two of these three components are zero, leaving just one none-zero component in the "out of the page" direction. In such case, magnetic field lines can be plotted as contours of the magnetic potential A or of the quantity, A^*, where:

$$A^* = \frac{A}{\sqrt{|A|}} \tag{6}$$

for a more detailed representation of a decaying magnetic field (e.g. close to the substrate holder).

The maximum radial magnetic field component B_ρ at the surface of a new 6.35 mm thick target reached a value of 550 G at a distance of 12.0 mm from the center, and the axial component B_z changed its direction at a distance $Z_0 = 13.1$ mm from the target surface. The level of unbalancing of the magnetron's magnetic field can be expressed by the unbalance coefficient, K, of the magnetron[29], defined as:

$$K = \frac{\Phi_o}{\Phi_i}, \tag{7}$$

where Φ_i and Φ_o denote magnetic fluxes from the inner and outer magnets on the target surface. In our case $K = 4.8$, while $K = 1$ for a perfectly balanced magnetron.

APPENDIX B

According to the model of Rossnagel,[4] the reduced Ar gas density n_r in front of the target caused by the flux of the sputtered material can be expressed as a function of the HD discharge current I_c as

$$n_r = \frac{-T_0 + (T_0^2 + \beta I_c)^{1/2}}{\gamma I_c}, \tag{8}$$

18

where

$$\beta = \frac{\overline{E_a}Y\sigma n_0 T_0}{\pi K_g f e} \tag{9}$$

and

$$\gamma = \frac{\overline{E_a}Y\sigma}{2\pi K_g f e}. \tag{10}$$

Here, n_0 and T_0 are the gas concentration and the gas temperature close to the chamber wall, $\overline{E_a}$ is the average energy of the sputtered particles, Y is the sputtering yield, σ is the collision cross section for momentum transfer, e is the elementary charge, K_g is the thermal conductivity of the gas, and f is a constant.

In order to calculate n_r from Eq. (8), the steady state HD current value corresponding to $U_c = 1.2\,\mathrm{kV}$ was used as an input parameter for the investigated target materials. A simplified assumption was used that the sputtering process is performed only by Ar ions. Furthermore, the cross section for momentum transfer σ was estimated by considering the "hard-sphere model" as

$$\sigma = \pi(a_s + a_g)^2, \tag{11}$$

where a_s and a_g are atomic diameters of sputtered and gas particles.[30] The sputtering yield Y and the average energy of sputtered atoms $\overline{E_a}$ were calculated using the TRIM computer program.[31] The value of the constant f was supposed to be 3, the wall temperature was $300\,\mathrm{K}$, the thermal conductivity of Ar gas K_g was $1.79 \times 10^{-2}\,\mathrm{W\,K^{-1}\,m^{-1}}$, and the pressure was $1\,\mathrm{Pa}$.
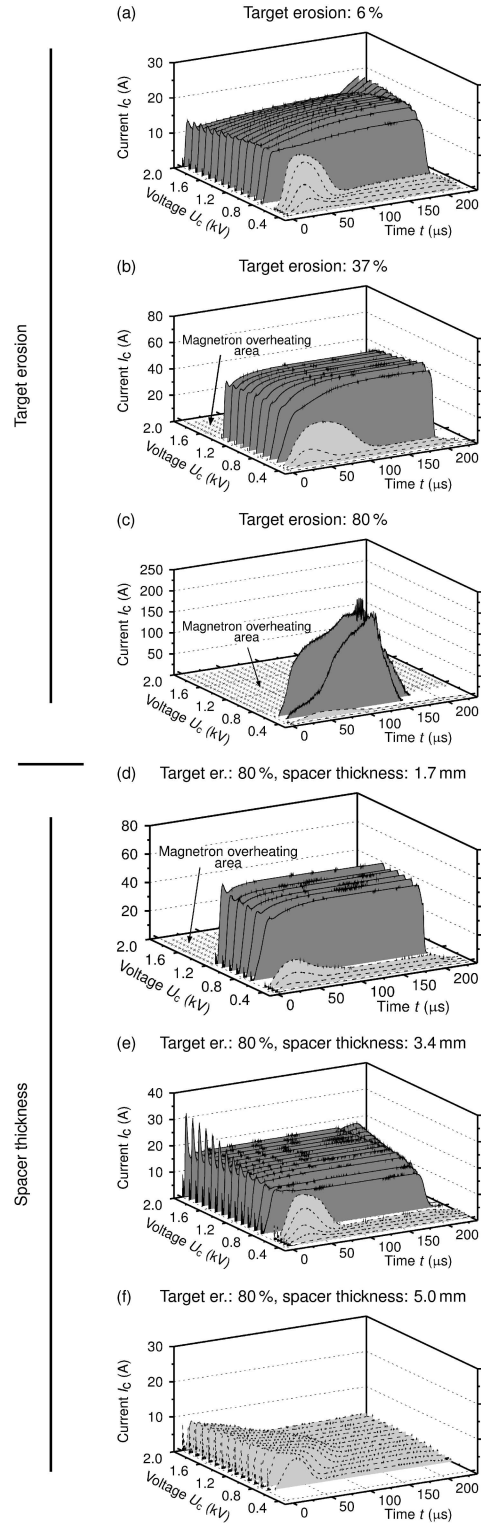
FIG. 7. Waveforms of the target current I_c as a function of a preset HiPIMS pulse voltage applied to a Nb target at different erosion states: 6 % (a), 37 % (b), and 80 % (c), and at 80 % of erosion state but for different thicknesses of spacers: 1.7 mm (d), 3.4 mm (e), and 5.0 mm (f).
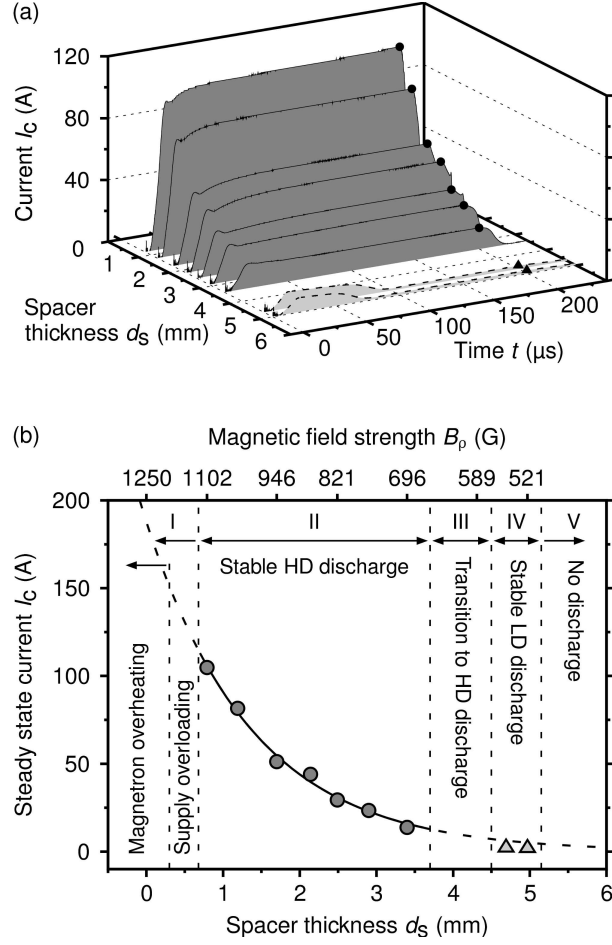
20

FIG. 8. Waveforms of the target current I_c at constant pulse voltage $U_c = 0.8\,\text{kV}$ as a function of the copper spacer thickness d_s positioned in between the Nb target (80 % of target erosion) and the magnetron head (a). The corresponding steady state current values I_c [at $t = 200\,\mu\text{s}$, as highlighted by solid symbols in (a)] are plotted as a function of the spacer thickness d_s, and various discharge modes are indicated (b).
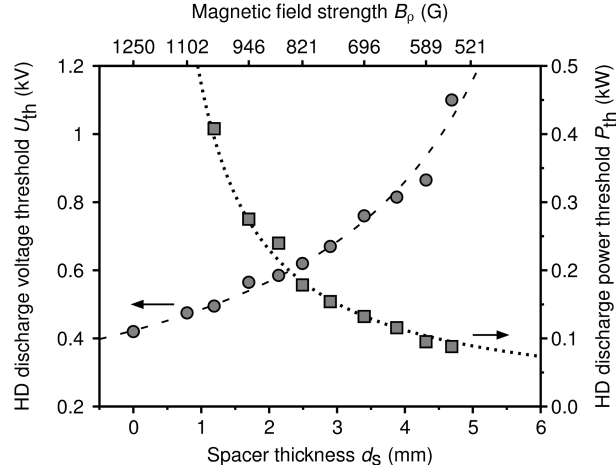
FIG. 9. Threshold U_{th} and corresponding minimum power P_{th} for the HD discharge as a function of the copper spacer thickness d_s positioned in between the Nb target (80 % of target erosion) and the magnetron head.
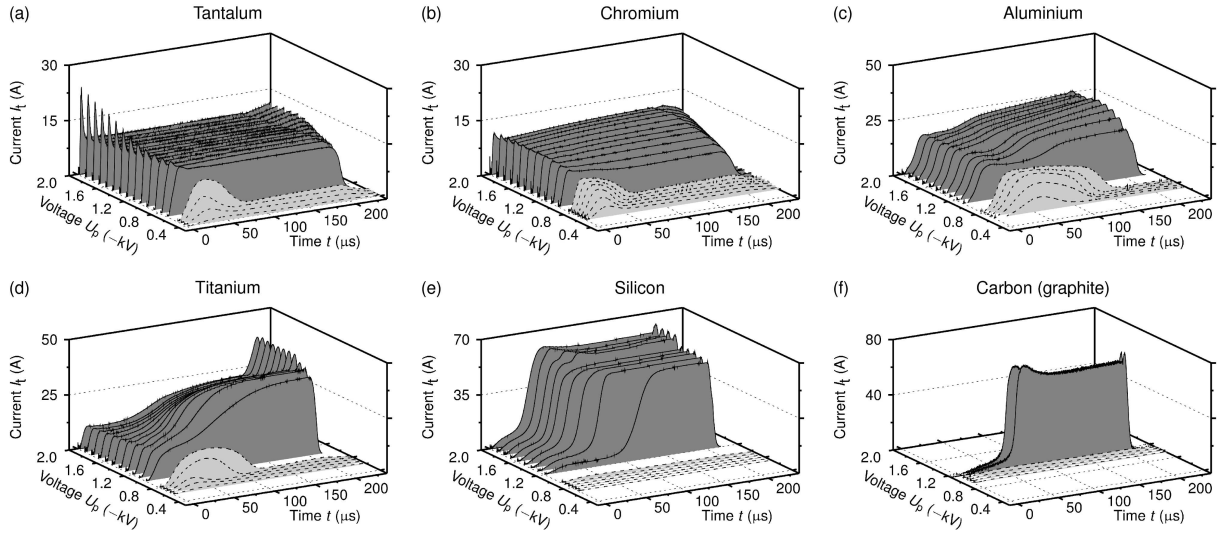

FIG. 10. Waveforms of the target current I_c as a function of the preset HiPIMS pulse voltage applied to different target materials: Ta (a), Cr (b), Al (c), Ti (d), Si (e), and C (f).
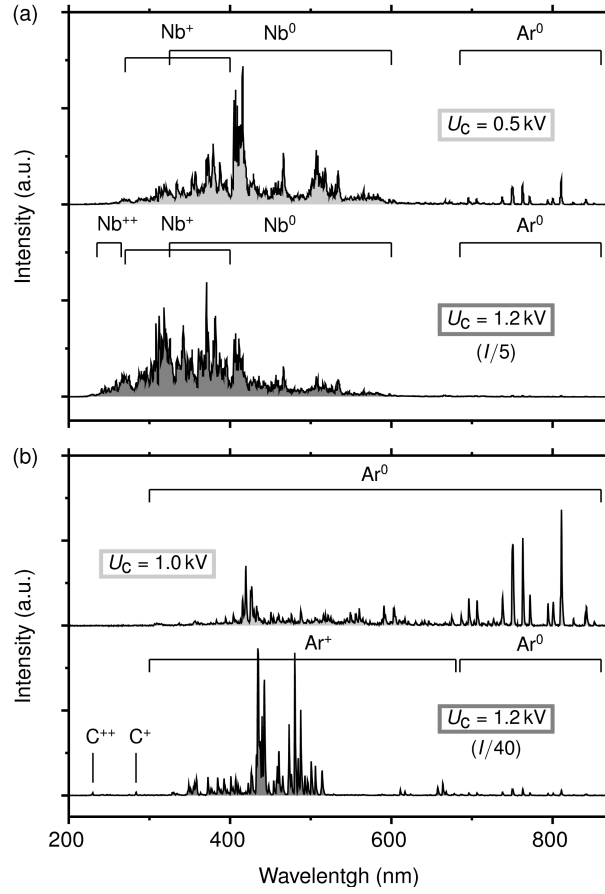
FIG. 11. Optical emission intensities from steady state LD (upper curves) and HD (lower curves) discharges operated above Nb (a) and C (b) targets. The optical emission probe was situated at $d = 1\,\mathrm{cm}$ from the target.
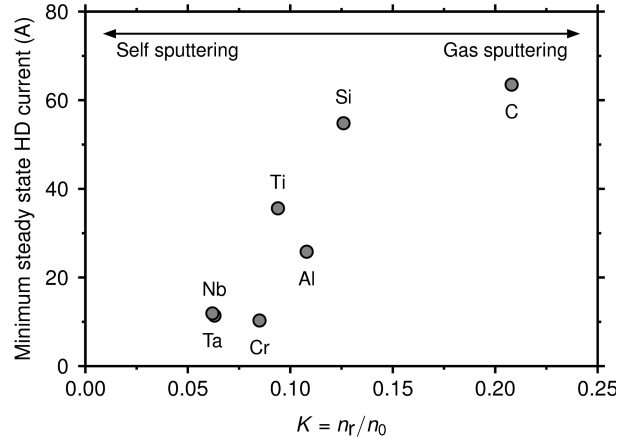
FIG. 12. Minimized steady state HD current at $U_c = 1.2\,\text{kV}$ as a function of the normalized density of the Ar gas in front of the target by sputtered particles of various materials (Ta, Nb, Cr, Al, Ti, Si, and C). The prevalent sputtering mechanisms are indicated.